Biomedical Optics EXPRESS

Hyperspectral and differential CARS microscopy for quantitative chemical imaging in human adipocytes

Claudia Di Napoli,[1] Iestyn Pope,[1] Francesco Masia,[2] Peter Watson,[1] Wolfgang Langbein,[2] and Paola Borri[1,*]

[1] *School of Biosciences, Cardiff University, Cardiff CF10 3US, UK*
[2] *School of Physics and Astronomy, Cardiff University, Cardiff CF24 3AA, UK*
[*] *borrip@cf.ac.uk*

Abstract: In this work, we demonstrate the applicability of coherent anti-Stokes Raman scattering (CARS) micro-spectroscopy for quantitative chemical imaging of saturated and unsaturated lipids in human stem-cell derived adipocytes. We compare dual-frequency/differential CARS (D-CARS), which enables rapid imaging and simple data analysis, with broadband hyperspectral CARS microscopy analyzed using an unsupervised phase-retrieval and factorization method recently developed by us for quantitative chemical image analysis. Measurements were taken in the vibrational fingerprint region (1200-2000/cm) and in the CH stretch region (2600-3300/cm) using a home-built CARS set-up which enables hyperspectral imaging with 10/cm resolution via spectral focussing from a single broadband 5 fs Ti:Sa laser source. Through a ratiometric analysis, both D-CARS and phase-retrieved hyperspectral CARS determine the concentration of unsaturated lipids with comparable accuracy in the fingerprint region, while in the CH stretch region D-CARS provides only a qualitative contrast owing to its non-linear behavior. When analyzing hyperspectral CARS images using the blind factorization into susceptibilities and concentrations of chemical components recently demonstrated by us, we are able to determine vol:vol concentrations of different lipid components and spatially resolve inhomogeneities in lipid composition with superior accuracy compared to state-of-the art ratiometric methods.

OCIS codes: (180.5655) Raman microscopy; (300.6230) Spectroscopy, coherent anti-Stokes Raman scattering.

References and links

1. A. Zumbusch, W. Langbein, and P. Borri, "Nonlinear vibrational microscopy applied to lipid biology," Prog. Lipid Res. **52**, 615–632 (2013).
2. J. P. Pezacki, J. A. Blake, D. C. Danielson, D. C. Kennedy, R. K. Lyn, and R. Singaravelu, "Chemical contrast for imaging living systems: molecular vibrations drive cars microscopy," Nat. Chem. Biol. **7**, 137–145 (2011).
3. M. Digel, R. Ehehalt, and J. Füllekrug, "Lipid droplets lighting up: Insights from live microscopy," FEBS Lett. **584**, 2168–2175 (2010).
4. T. C. Walther and R. V. Farese Jr, "Lipid droplets and cellular lipid metabolism," Annu. Rev. Biochem. **81**, 687–714 (2012).
5. S. Fukumoto and T. Fujimoto, "Deformation of lipid droplets in fixed samples," Histochem. Cell Biol. **118**, 423–428 (2002).

#206105 - $15.00 USD Received 11 Feb 2014; revised 9 Mar 2014; accepted 9 Mar 2014; published 2 Apr 2014

6. X. Nan, J. X. Cheng, and X. S. Xie, "Vibrational imaging of lipid droplets in live fibroblast cells with coherent anti-stokes raman scattering microscopy," J. Lipid Res. **44**, 2202–2208 (2003).
7. Y. Ohsaki, Y. Shinohara, M. Suzuki, and T. Fujimoto, "A pitfall in using bodipy dyes to label lipid droplets for fluorescence microscopy," Histochem. Cell Biol. **133**, 477–480 (2010).
8. M. Paar, C. Jüngst, N. A. Steiner, C. Magnes, F. Sinner, D. Kolb, A. Lass, R. Zimmermann, A. Zumbusch, S. D. Kohlwein, and H. Wolinski, "Remodeling of lipid droplets during lipolysis and growth in adipocytes," J. Biol. Chem. **287**, 11164–11173 (2012).
9. E. M. Vartiainen, H. A. Rinia, M. Müller, and M. Bonn, "Direct extraction of raman line-shapes from congested cars spectra," Opt. Express **14**, 3622–3630 (2006).
10. Y. Liu, Y. J. Lee, and M. T. Cicerone, "Broadband cars spectral phase retrieval using a time-domain kramers-kronig transform," Opt. Lett. **34**, 1363–1365 (2009).
11. H. A. Rinia, K. N. J. Burger, M. Bonn, and M. Müller, "Quantitative label-free imaging of lipid composition and packing of individual cellular lipid droplets using multiplex cars microscopy," Biophys. J. **95**, 4908–4914 (2008).
12. I. Rocha-Mendoza, W. Langbein, P. Watson, and P. Borri, "Differential coherent anti-stokes raman scattering microscopy with linearly-chirped femtosecond laser pulses," Opt. Lett. **34**, 2258–2260 (2009).
13. W. Langbein, I. Rocha-Mendoza, and P. Borri, "Single source coherent anti-stokes raman microspectroscopy using spectral focusing," Appl. Phys. Lett. **95**, 081109 (2009).
14. I. Rocha-Mendoza, P. Borri, and W. Langbein, "Quadruplex cars micro-spectroscopy," J. Raman Spectr. **44**, 255–261 (2013).
15. C. Di Napoli, F. Masia, I. Pope, C. Otto, W. Langbein, and P. Borri, "Chemically-specific dual/differential cars micro-spectroscopy of saturated and unsaturated lipid droplets," J. Biophotonics **7**, 68–76 (2014 (2012 online)).
16. F. Masia, A. Glen, P. Stephens, P. Borri, and W. Langbein, "Quantitative chemical imaging and unsupervised analysis using hyperspectral coherent anti-stokes raman scattering microscopy," Anal. Chem. **85**, 10820–10828 (2013).
17. I. Pope, W. Langbein, P. Watson, and P. Borri, "Simultaneous hyperspectral differential-CARS, TPF and SHG microscopy with a single 5 fs ti:sa laser," Opt. Express **21**, 7096–7106 (2013).
18. T. Hellerer, A. M. Enejder, and A. Zumbusch, "Spectral focusing: High spectral resolution spectroscopy with broad-bandwidth laser pulses," Appl. Phys. Lett. **85**, 25–27 (2004).
19. I. Rocha-Mendoza, W. Langbein, and P. Borri, "Coherent anti-stokes raman microspectroscopy using spectral focusing with glass dispersion," Appl. Phys. Lett. **93**, 201103 (2008).
20. L. L. Listenberger and D. A. Brown, "Fluorescent detection of lipid droplets and associated proteins," Curr. Protoc. Cell Biol. **24.2**, 24.2.1–24.2.11 (2007).
21. L. Hodson, C. M. Skeaff, and B. A. Fielding, "Fatty acid composition of adipose tissue and blood in humans and its use as a biomarker of dietary intake," Progress in Lipid Research **47**, 348–380 (2008).
22. D. Gachet, F. Billard, N. Sandeau, and H. Rigneault, "Coherent anti-Stokes Raman scattering (CARS) microscopy imaging at interfaces: evidence of interference effects" Opt. Express **15**, 10408–10420 (2007).
23. A. M. Barlow, K. Popov, M. Andreana, D. J. Moffatt, A. Ridsdale, A. D. Slepkov, J. L. Harden, L. Ramunno, and A. Stolow, "Spatial-spectral coupling in coherent anti-Stokes Raman scattering microscopy" Opt. Express **21**, 15298–15307 (2013).

1. Introduction

Optical microscopy is an indispensable tool that is driving progress in cell biology, and is still the only practical means of obtaining spatial and temporal resolution within living cells and tissues. Coherent anti-Stokes Raman scattering microscopy has emerged in the last decade as a multiphoton technique able to image living cells label-free in real time with high three-dimensional spatial resolution and chemical specificity [1, 2]. CARS is a third-order nonlinear process where molecular vibrations are coherently driven by the interference between two optical fields (pump and Stokes) and a third field (the pump itself in a two-pulse CARS system) is used to generate anti-Stokes Raman scattering from the driven vibrations. Owing to the coherence of the driving process, CARS benefits, unlike spontaneous Raman, from the constructive interference of light scattered by spectrally overlapping vibrational modes within the focal volume, thus enabling fast acquisition at moderate powers compatible with live cell imaging. Being a nonlinear process, CARS is generated only in the focal volume where high photon densities are reached, allowing for an intrinsic 3D spatial resolution (optical sectioning) similar to other multiphoton microscopy techniques such as two-photon fluorescence and second-harmonic generation.

#206105 - $15.00 USD Received 11 Feb 2014; revised 9 Mar 2014; accepted 9 Mar 2014; published 2 Apr 2014

CARS microscopy has proven to be particularly successful in imaging unstained lipids especially when concentrated in vesicles such as cytosolic lipid droplets (LDs), owing to the large number of identical CH bonds in the lipid acyl chain. LDs are found in many cell types and consist of a hydrophobic core containing neutral lipids, mainly triglycerides and sterol esters, surrounded by a phospholipid monolayer. During the last two decades, it has become apparent that cytosolic LDs are highly dynamic organelles beyond static energy deposits, and are involved in the fine regulation of lipid metabolism and in turn the pathophysiology of metabolic diseases such as atherosclerosis, diabetes and obesity [3, 4]. The recent development of CARS micro-spectroscopy has further boosted this interest by opening the prospect to image LDs in living cells with an unprecedented intrinsic chemical specificity and without introducing staining artifacts. Such artifacts include for example cytosolic LD fusion artificially induced by standard staining protocols [5–7]. Recently, it became possible to gain detailed quantitative insights about the fusion behavior of unstained LDs in adipocytes with CARS time-course experiments over more than a week on the same cells without the limitation of marker bleaching [8].

Among the various technical implementations of CARS microscopy reported to date, hyperspectral CARS imaging is receiving increasing attention due to its superior chemical specificity compared to single-frequency CARS. In hyperspectral CARS, a CARS spectrum is measured at each spatial position, either by taking a series of spatially-resolved images at different vibrational frequencies, or by acquiring a spectrum at each spatial point following simultaneous excitation of several vibrations (the latter is also called multiplex CARS). Since the CARS intensity is proportional to the absolute square of the third-order susceptibility it contains the interference between vibrationally resonant and non-resonant terms and results in a non-trivial lineshape and dependence on the concentration of chemical components. In hyperspectral CARS, this limitation can be overcome by acquiring CARS intensity spectra over a sufficiently wide spectral range and analyzing them to retrieve Raman-like spectra linear in the concentration of chemical components [9, 10].

Multiplex CARS microscopy has previously been used to monitor the composition of LDs in differentiated mouse adipocytes (3T3-L1 cells) under different dietary conditions [11]. In Ref. [11], CARS spectra were analyzed using the maximum entropy method to derive the imaginary part of the CARS susceptibility resulting in Raman-like spectra. Ratios between amplitudes of these retrieved spectra at different vibrational resonances were then used to infer information about the acyl-chain order and the ratio between saturated and unsaturated fatty acids. This approach allowed the identification of variations in the composition of LDs in individual cells. However, measurements had to be taken on fixed cells since multiplex CARS typically requires acquisition times of ~ 10 ms per spectrum and in turn tens of minutes for the acquisition of spatially-resolved 3D images.

We recently demonstrated a method named dual-frequency/differential CARS (D-CARS) micro-spectroscopy where two vibrational frequencies are excited and probed simultaneously, and the sum and difference between the corresponding CARS intensities is detected by a single-channel fast photomultiplier using phase-sensitive frequency filtering [12–14]. This provides improved chemical specificity compared to single-frequency CARS and rejection of the spectrally-constant non-resonant CARS background without significant post-acquisition data analysis, while maintaining the high imaging speed of single-frequency CARS compatible with live cell imaging. We recently demonstrated the applicability of this method to distinguish in a rapid label-free way the chemical composition of micron-sized lipid droplet model systems consisting of pure triglycerides types (saturated and unsaturated) in an agarose gel [15]. However the question whether the technique would be able to distinguish different lipid compositions in a more complex chemical scenario such as LDs in cells remained open. We also recently demonstrated a novel method to analyze hyperspectral CARS microscopy images of organic

#206105 - $15.00 USD Received 11 Feb 2014; revised 9 Mar 2014; accepted 9 Mar 2014; published 2 Apr 2014

materials and biological samples resulting in an unsupervised and unbiased quantitative chemical analysis, which we named blind factorization into susceptibilities and concentrations of chemical components (FSC^3) [16].

In the present work, we have investigated the chemical composition of LDs in human adipose-derived stem cells (ADSCs) cultured with known supplemented mixtures of saturated and unsaturated fatty acids. We used both D-CARS and hyperspectral CARS microscopy in the vibrational fingerprint region (1200-2000/cm) and in the CH stretch region (2600-3300/cm) with FSC^3 data analysis, and quantitatively assessed and compared the capabilities of both techniques in this chemically-complex biologically relevant scenario.

2. Materials and methods

2.1. CARS micro-spectroscopy set-up

Hyperspectral CARS and D-CARS images were acquired with a home-built set-up based on a single Ti:Sapphire 5 fs broadband (660-970 nm) laser system as described in detail in Ref. [17]. Briefly, pump and Stokes components for the CARS excitation are obtained by spectrally separating the broadband laser output with an appropriate sequence of dichroic beam splitters, resulting in a pump (Stokes) with center wavelength at 682 nm (806 nm) and a bandwidth of 65 nm (200 nm). A spectral resolution of 10/cm is achieved through spectral focusing [18], namely an equal linear chirp applied to pump and Stokes in order to maintain a constant instantaneous frequency different (IFD) through the stretched pulse duration, using SF57 glass blocks of appropriate length [19]. We perform CARS spectroscopy rapidly without adjustments to the laser by simply changing the relative delay time t_0 between pump and Stokes pulses which results in a tuning of the IFD across the entire 1200-3800/cm vibrational range, owing to the large bandwidth of the Stokes pulse. D-CARS is implemented as described in our previous works [12, 17]. In this technique, the pump-Stokes pair is divided into two orthogonally polarized pairs, Π_1 and Π_2, with Π_2 travelling through an additional thin SF57 glass element and delayed by half the laser repetition period relative to Π_1. When the two pairs are recombined, a pulse sequence at twice the laser repetition rate is created where Π_1 excites the vibrational resonance ν_{IFD1} adjustable through t_0 and Π_2 excites the shifted resonance $\nu_{\mathrm{IFD2}} = \nu_{\mathrm{IFD1}} - \Delta_{\mathrm{IFD}}$ with the frequency difference Δ_{IFD} being determined by the thickness of the additional SF57 glass. By frequency analyzing the CARS signal, we can simultaneously detect the dc component proportional to the sum of the CARS intensity from Π_1 and Π_2 and the ac component at the pulse repetition rate proportional to the difference of the CARS intensity from Π_1 and Π_2. The excitation pulses were coupled into a commercial inverted microscope stand (Nikon Ti-U) via a home-built beam-scanning head. The microscope is equipped with a 20x 0.75 NA dry objective (Nikon CFI Plan Apochromat λ series) and the CARS signal is collected in forward direction with a 0.72 NA dry condenser, frequency selected by appropriate band-pass filters and detected by a photomultiplier tube (Hamamatsu H7422-40). The resulting CARS spatial resolution (FWHM of the intensity point-spread function) was measured to be 0.6 μm and 1.1 μm in the lateral (*xy*) and axial (*z*) direction, respectively [17]. A motorized sample stage enabled *xy* sample movement and a motorized objective focussing enabled *z* movement (Prior ProScan III).

The microscope stand was also equipped with differential interference contrast (DIC) optics and cells of interest were first identified with DIC. CARS hyperspectral *xy* images were acquired in the fingerprint region (1200-2000/cm) and in the CH region (2600-3300/cm) with 5/cm spectral steps. The reason for acquiring the two ranges separately is two-fold, as detailed in our previous work [17]. Firstly, non-linear chirp affecting the broadband Stokes pulse implies that the chirp on this pulse can be approximated as linear only for a limited wavelength range and thus requires different lengths of SF57 glass blocks to match the pump chirp at dif-

#206105 - $15.00 USD Received 11 Feb 2014; revised 9 Mar 2014; accepted 9 Mar 2014; published 2 Apr 2014

ferent Stokes centre wavelengths. Secondly, different detection bandwidth filters are needed for the two ranges, as shown in Table 1 in Ref. [17]. D-CARS *xy* images were acquired at wavenumbers maximizing the chemical contrast [15], as indicated in each figure. *xy* images were acquired using beam scanning with a pixel size of $0.3\times0.3\,\mu m^2$ and a pixel dwell time of $10\,\mu s$, resulting in 1.6 s acquisition time for a $120\times120\,\mu m^2$ single-frequency or D-CARS image. Correspondingly, a typical hyperspectral image stack with 100 spectral points required a total acquisition time of 160 s (less than 3 min). Images were acquired at a fixed *z* determined as the axial position for which most medium-sized (3-5 μm diameter) LDs are equatorially cut such that the lipid content of their inner core is optimally imaged. Non-resonant CARS spectra from glass were also recorded and used for normalization (i.e. measured CARS intensities in each sample were divided by the corresponding non-resonant CARS intensity in glass under the same excitation and detection conditions) in order to correct for the varying temporal overlap of pump and Stokes and to derive a CARS intensity ratio independent of excitation/detection parameters [15, 16]. All experiments were performed at room temperature.

2.2. Cell samples

Human ADSCs (Invitrogen) were cultured in low glucose Dulbecco's modified eagle medium and GlutaMAX™ supplemented with 10% mesenchymal stem cells qualified FBS, $75\,\mu g$/mL Gentamicin and $37.5\,\mu g$/mL Amphotericin. In order to induce differentiation into adipocytes, ADSCs were grown in StemPro® (Invitrogen) adipogenic differentiation media in accordance with the manufacturer's protocol. After 3 days, the medium was supplemented with a fatty acid-BSA complex resulting in $9.4\,\mu g$/mL of supplemented fatty acid in the final medium. Palmitic acid (PA) and α-linolenic acid (LA) complexes were prepared in house [20] with PA and LA purchased from Sigma-Aldrich. Structurally, PA is a saturated 16-carbon chain (*hexadecanoic acid*) and LA is a tri-unsaturated 18-carbon chain with *cis* double bonds at the 9, 12, and 15th position from the first carbon atom (*cis,cis,cis-9,12,15-octadecatrienoic acid*). Cells were grown for 3 additional days in the supplemented medium and then fixed in 4% formaldehyde-PBS solution. After fixation, coverslips containing cells were mounted onto standard glass slides using 120 μm thick imaging gaskets (Grace Bio-lab SecureSeal™) filled with water.

2.3. Data analysis

CARS and D-CARS images were background-corrected by subtracting an image measured under identical excitation/detection conditions but with pump and Stokes pulses out of time overlap. Note that, by simultaneous detection in the epi-direction [17], we could rule out the presence of a significant background arising from pump-Stokes two-photon absorption (which would be dependent on their time overlap) hence this background subtraction procedure is appropriate. Hyperspectral images were noise-filtered with a singular value decomposition (SVD) algorithm on the square root of the CARS intensity to retain only components above noise, as described in our recent work [16]. CARS intensity ratios were calculated by dividing the background-corrected CARS intensity by the corresponding non-resonant CARS intensity measured in glass under the same excitation and detection conditions. The phase-corrected Kramers-Kronig method [16] (PCKK) was used to retrieve from the CARS intensity ratio the complex CARS third-order susceptibility (normalized to the non-resonant value in glass) which is linear in the concentration of chemical components, and in particular its imaginary part $\Im(\tilde{\chi})$. We then used non-negative matrix factorization applied to the imaginary part and the non-resonant real part of the susceptibility with an additional concentration constraint (blind factorization into susceptibilities and concentrations of chemical components -FSC^3 method) to obtain susceptibility spectra of independently varying chemical components and their vol-

#206105 - $15.00 USD Received 11 Feb 2014; revised 9 Mar 2014; accepted 9 Mar 2014; published 2 Apr 2014

ume concentration [16]. As well as representing the full spatial distribution of CARS intensity ratios, the retrieved $\Im(\bar{\tilde{\chi}})$ and the associated spatial maps of independently varying chemical components, we also calculated LD mean spectra by averaging spectra over more than 100 LDs for each group of cells fed with the same fatty acids (each group containing at least 6 differentiated cells). In this case only LDs with a diameter above 2 μm were considered, and the spectrum of each LD was taken by averaging over the LD core spatial region of constant CARS intensity, to take into account only regions completely filled with lipids.

3. Results and discussion

3.1. Hyperspectral CARS

Hyperspectral images of CARS intensity ratios and the corresponding phase-retrieved imaginary part $\Im(\bar{\tilde{\chi}})$ are shown in Fig. 1 for human ADSCs grown in media supplemented with either saturated (palmitic) or unsaturated (α-linolenic) fatty acids. Images are shown at characteristic wavenumbers, and full spectra are given as averages over more than 100 LDs of spatially well resolved size. The CARS intensity ratio has a spectral shape affected by the interference between the resonant vibrational contribution and the non-resonant electronic contribution to the CARS susceptibility resulting in a dispersive lineshape in the fingerprint region and a spectral shape only qualitatively resembling a Raman spectrum in the CH stretch region. A Raman-like spectrum is recovered in the retrieved $\Im(\bar{\tilde{\chi}})$ exhibiting the characteristic vibrational bands typical of neutral lipids [15]. In the fingerprint region bands are observed at around 1450/cm due to CH_2 and CH_3 deformations and at 1660/cm due to the C=C stretch vibration which is absent in saturated lipids. The weak band around 1740/cm is attributed to the C=O stretch from the ester bonds between glycerol and the fatty acids and demonstrates the storage of lipids in the form of triglycerides [15]. The CH stretch region is more congested with several overlapping resonances. The most prominent features are the band at around 2850/cm from the CH_2 symmetric stretch vibrational resonance and the broad shoulder at around 2930/cm which is a combination of CH_3 stretch vibrations and CH_2 asymmetric stretch enhanced by the broadening and shift of the CH deformations in the liquid phase. Polyunsaturated lipids which are liquid at room temperature exhibit a significant band around 2930/cm. The =CH stretch gives rise to a band around 3010/cm. We clearly observe that cells fed with LA which is poly-unsaturated have on average much more prominent bands at 1660/cm, 2930/cm and 3010/cm characteristic of the presence of unsaturated bonds compared to cells fed with PA. Noticeably, the retrieved spectrum of $\Im(\bar{\tilde{\chi}})$ for these cells has a similar shape to the Raman spectrum of pure α-glyceryl trilinolenate [15] (particularly the relative amplitude between the 1660/cm and 1450/cm bands) indicating an efficient uptake and storage of LA in these samples. This is consistent with other findings in the literature indicating that the different fatty-acid composition in the medium does change the chemical composition of LDs in adipocytes [11]. Conversely, cells fed with PA still show the presence of unsaturated bonds. The average LD spectrum in these cells is similar to that measured for oleic acid [15, 16] which appears to be the main fatty acid component of the differentiation medium (cells grown in a medium supplemented with oleic acid also showed very similar spectra, data not shown). This suggests that under our experimental conditions, human ADSCs incorporate LA much more efficiently than PA. This point is discussed in greater detail in a following section.

3.2. Dual-frequency differential CARS

In a previous work we demonstrated that D-CARS, measuring the difference between the CARS intensity at suitable wavenumbers, is a tool to suppress the non-resonant background and perform chemically-discriminative imaging with fast acquisition speeds on LD model sys-

#206105 - $15.00 USD Received 11 Feb 2014; revised 9 Mar 2014; accepted 9 Mar 2014; published 2 Apr 2014

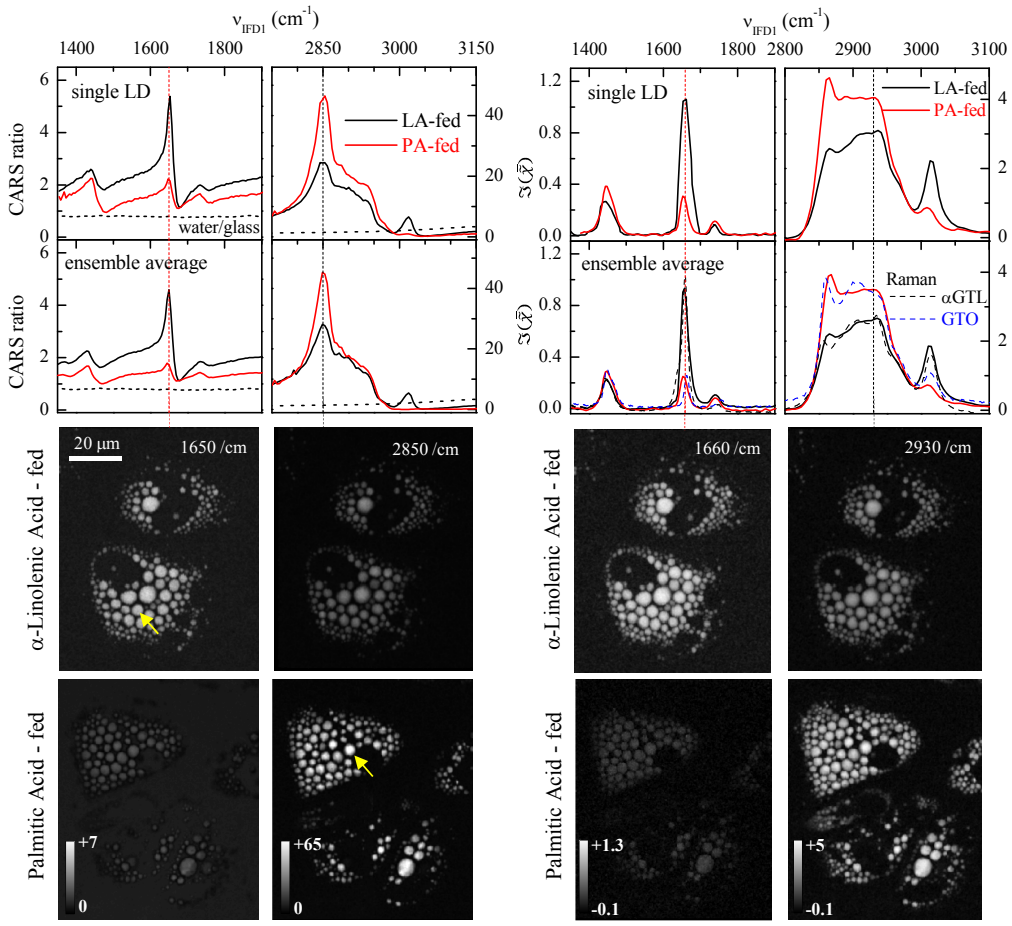

Fig. 1. CARS intensity ratio (left) and phase-retrieved imaginary part of the normalized susceptibility $\Im(\tilde{\chi})$ (right). Images (lower panels) as well as spectra (upper panels) averaged over more than 100 LDs, and for the individual droplet indicated by the yellow arrow, are shown for human adipose-derived stem cells fed with palmitic acid (PA) and α-linolenic acid (LA). Raman spectra of α-glyceryl trilinolenate (αGTL) and glyceryl trioleate (GTO) are shown for comparison (dashed lines). In the CARS intensity ratio, the spectrum of the water to glass ratio is also shown. Images of the CARS intensity ratio are shown at 1650/cm and 2850/cm, as indicated by the vertical dotted lines in the spectra. Images of the imaginary part of the normalized susceptibility are shown at 1660/cm and 2930/cm. Linear grey scales are indicated. The pump power on the sample was 20 mW (14 mW) and the Stokes power was 10 mW (7 mW) for the fingerprint region (CH region); 10 μs pixel dwell time, 0.3 μm pixel size.

tems [15]. The purpose of this study is to investigate the validity of this technique in a more physiologically relevant but chemically complex case such as cytosolic LDs in adipocytes.

The D-CARS results corresponding to Fig. 1 are given in Fig. 2. The upper panel shows simulated D-CARS spectra constructed using the single-pair CARS intensity ratio of Fig. 1 and the experimental value of the wavenumber shift Δ_{IFD}. As described in detail in Ref. [15], we construct a shifted spectrum to represent the effect of the second pulse pair in the D-CARS experiment and calculate the difference accordingly. These calculations agree well with ex-

#206105 - $15.00 USD Received 11 Feb 2014; revised 9 Mar 2014; accepted 9 Mar 2014; published 2 Apr 2014

perimentally measured D-CARS spectra [15]. The experimental D-CARS images measured at selected wavenumbers are shown in the lower panels of Fig. 2.

In the fingerprint region, D-CARS images were measured for $\Delta_{\mathrm{IFD}} = 34$/cm. This value was chosen to provide the maximum D-CARS contrast since it is comparable to the wavenumber distance from the peak to the dip in the dispersive lineshape of the CARS ratio at around 1450/cm and 1660/cm. The simulated D-CARS spectra have a maximum at around 1470/cm and 1680/cm for which D-CARS images were acquired. The peak at 1680/cm is a measure of the abundance of the C=C stretch band in the LDs of cells fed with α-linolenic acid.

In the more congested CH region, D-CARS images were measured using $\Delta_{\mathrm{IFD}} = 65$/cm which enables distinction of saturated from poly-unsaturated triglycerides based on their different CARS intensity lineshapes and relative importance of the peak at 2850/cm and the broad shoulder at around 2930/cm, as discussed in details in Ref. [15]. Simulated D-CARS spectra have a maximum at around 2920/cm, which is more pronounced for cells fed with PA consistent with the presence of more saturated or mono-unsaturated fatty acids compared to cells fed with LA. D-CARS images are shown at 2920/cm and at 2990/cm for relative comparison (with D-CARS at 2990/cm being a measure of the amplitude of the broad shoulder in the CARS intensity spectrum, see sketch in Fig. 2). For the CARS intensity peak around 3010/cm characteristic of the =CH bond, D-CARS was acquired using $\Delta_{\mathrm{IFD}} = 27$/cm comparable to the linewith of this peak. Simulated D-CARS spectra show a maximum at 3045/cm proportional to the amplitude of this CARS intensity peak. Corresponding D-CARS images measured at 3045/cm show the presence of this peak for cells fed with LA.

We note that, although it might appear cumbersome to use different Δ_{IFD} in the D-CARS technique, the choice of which might not be straightforward without an a priori knowledge of the substance to be investigated, an approach which can be taken as a general rule for D-CARS is to use Δ_{IFD} comparable to the resonance linewidth.

3.3. Ratiometric analysis

As shown by Rinia *et al.* [11] a ratiometric analysis can be used to quantitatively determine the degree of C=C polyunsaturation and the order of lipids (i.e. their fluidity) in cytosolic LDs. In particular, the ratio of the phase-retrieved $\Im(\tilde{\chi})$ between 1660/cm and 1450/cm was shown to provide a quantitative measure for the degree of lipid-chain unsaturation. The ratio of $\Im(\tilde{\chi})$ between the band at around 2930/cm and the CH_2 symmetric stretch resonance at 2850/cm can be used as a measure of the disorder [15]. In Fig. 3 we show this ratiometric analysis performed both for D-CARS and the phase-retrieved $\Im(\tilde{\chi})$. Human ADSCs were fed with media supplemented with PA, LA and their mixtures. For each group of cells fed with one type of lipid-supplemented medium, the ratio was calculated on more than 100 LDs of resolved diameter and the average ratio together with its standard deviation in the statistics are shown as symbols and error bars in Fig. 3.

In the fingerprint region, the ratio measured using D-CARS coincides within errors with the ratio using $\Im(\tilde{\chi})$ and scales proportionally to the LA volume fraction used in the experiments (the dashed line in Fig. 3 shows the linear dependence proportional to the LA volume fraction). Since $\Im(\tilde{\chi})$ is linear in the concentration of chemical components [16], this result demonstrates that i) on average the cellular uptake of LA in the lipid droplets of ADSCs follows the LA relative concentration in the supplemented medium and ii) D-CARS is equally able to quantitatively determine the degree of C=C poly-unsaturation in cytosolic LDs, circumventing hyperspectral CARS measurements and data analysis. In the CH stretch region, $\Im(\tilde{\chi})$ ratios scale linearly with the LA volume fraction used in the experiments (see dashed lines), as expected from the linearity of the phase-retrieved imaginary part of the susceptibility. Conversely, D-CARS ratios are different from $\Im(\tilde{\chi})$ ratios and whilst showing a qualitatively similar trend to $\Im(\tilde{\chi})$ as a

#206105 - $15.00 USD Received 11 Feb 2014; revised 9 Mar 2014; accepted 9 Mar 2014; published 2 Apr 2014

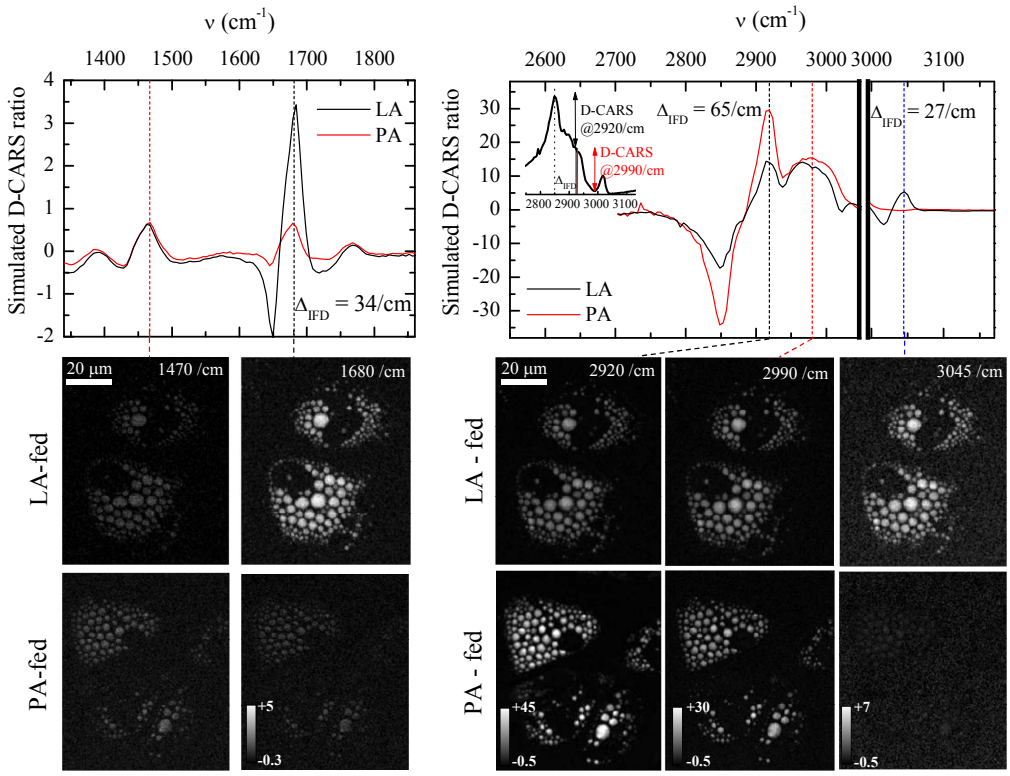

Fig. 2. D-CARS imaging in the fingerprint and CH region of human ADSCs fed with different fatty acids as given in Fig. 1. Top: D-CARS spectra calculated from the measured CARS intensity ratios shown in Fig. 1 with Δ_{IFD} as indicated. In the CH stretch region, the inset schematically shows D-CARS amplitudes (vertical arrows) at 2920/cm and 2990/cm in relation to the CARS intensity linshape. Bottom: D-CARS images of adipocytes measured at the wavenumbers indicated by corresponding dotted lines (1470 and 1680/cm in the fingerprint region; 2920, 2990 and 3045/cm in the CH region) on a grey scale as shown. Pump power on each pair 16 mW, Stokes power on each pair 8 mW, 10 μs pixel dwell time, 0.3 μm pixel size.

function of the lipid mixture they exhibit significant quantitative deviations. This is due to the non-linear concentration dependence of CARS which is retained in D-CARS in the CH stretch region.

3.4. *Quantitative chemical analysis using FSC*^{3}

A key point in CARS micro-spectroscopy is the determination of the spatial distribution of chemical components. Hence, beside calculating D-CARS and $\Im(\bar{\chi})$ as average values over many LDs as shown in Fig. 3, we want to address the question of what is the spatially-resolved chemical composition of LDs even within cells fed with one type of lipid. The error bars in the ratios of $\Im(\bar{\chi})$ in Fig. 3 give us a measure of the distribution width in the degree of unsaturation and lipid order in the investigated LD ensembles, and suggest fairly homogeneous distributions in most cases. They also include measurement noise, which is however not significant for the observed distribution width, also due to the noise filtering [16] with SVD. A much more detailed picture is obtained using the FSC^3 method [16].

#206105 - $15.00 USD Received 11 Feb 2014; revised 9 Mar 2014; accepted 9 Mar 2014; published 2 Apr 2014

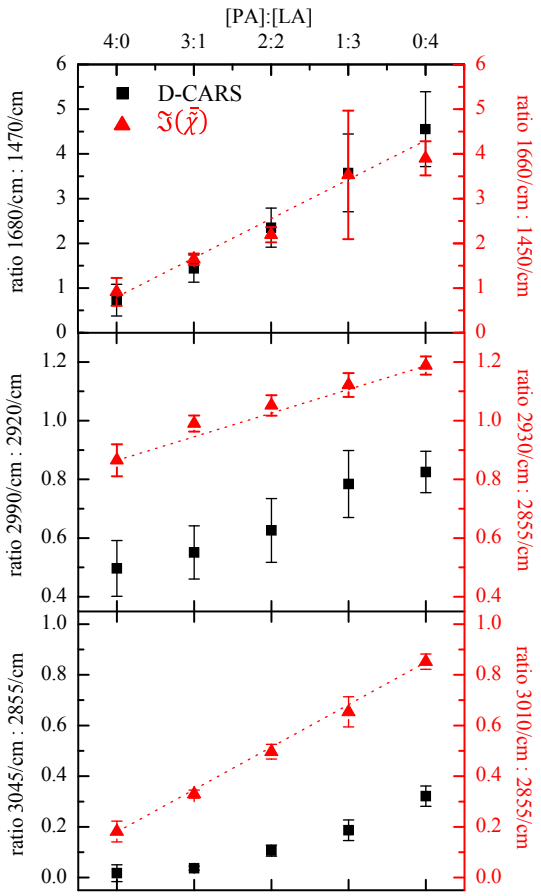

Fig. 3. Ratiometric analysis of measured D-CARS ratio and phase-retrieved $\Im(\bar{\chi})$ in human ADSCs fed with mixtures of palmitic acid and α-linolenic acid with a vol:vol ratio as indicated. Black squares give average D-CARS intensity ratios, red triangles give average ratios of $\Im(\bar{\chi})$. The errors bars show the standard deviation over the analyzed droplets ensemble. Dotted lines are the calculated linear dependencies according to the mixture ratio from the values with pure PA and LA. Top: D-CARS ratio between 1680/cm and 1470/cm and corresponding ratio of $\Im(\bar{\chi})$ at 1660/cm and 1450/cm. Middle: D-CARS intensity ratio between 2990/cm and 2920/cm and corresponding ratio of $\Im(\bar{\chi})$ at 2930/cm and 2855/cm. Bottom: D-CARS intensity ratio between 3045/cm and 2855/cm and corresponding ratio of $\Im(\bar{\chi})$ at 3010/cm and 2855/cm.

Fig. 4 shows the FSC^3 results on the investigated human ADSCs fed with PA, LA and the equal volume mixture of both. In this analysis we considered 5 chemical components which was the minimum number needed to well represent the chemical composition of all samples. Their spectral profile and spatial distribution in volume concentration units is shown in the figure. The component number 1 with the highest volume fraction in all samples is water (shown in Fig. 4 for cells fed with LA). The main lipid component of medium-large sized cytosolic LDs appears as component 4 in the analysis and has the same characteristic spectrum as shown in Fig. 1. Its spatial distribution is color–coded in red in the red–green–blue (RGB) overlay of Fig. 4. Moreover, a chemical component spatially located in the cytosol and the nucleus is distinguished (component 3, spatial distribution color–coded in blue), with a spectrum having a

#206105 - $15.00 USD Received 11 Feb 2014; revised 9 Mar 2014; accepted 9 Mar 2014; published 2 Apr 2014

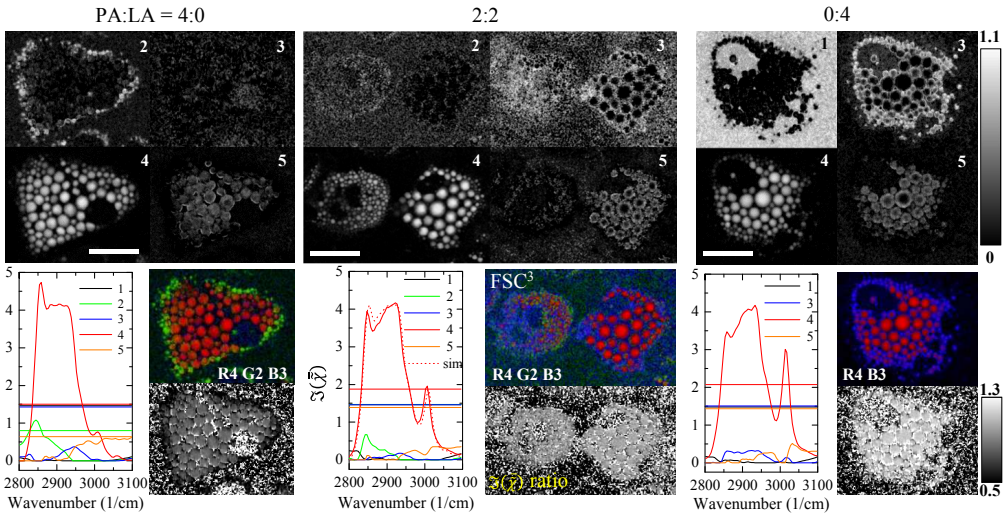

Fig. 4. Results of FSC^3 on the phase-retrived $\Im(\bar{\tilde{\chi}})$ in human ADSCs fed with PA, LA and an equal mixture (vol:vol) of PA and LA. Top: Spatial distributions of the volume concentration on a gray scale from 0 (black) to 1.1 (white) for the 5 components considered in the analysis. Bottom: spectra of $\Im(\bar{\tilde{\chi}})$ and its real part (horizontal lines) for the corresponding components. In the spectra for the PA:LA mixture the thin dotted line is an equally weighted superposition from component 4 of cells fed with PA and LA only. RGB overlays show the spatial distribution of the concentration for specific components as indicated. Below the RGB overlays, the spatial distribution of the $\Im(\bar{\tilde{\chi}})$ ratio between 2930/cm and 2855/cm is shown on a gray scale, as indicated. The scale bars indicate 20 μm.

pronounced band at around 2930/cm characteristic of proteins and nucleic acids (partly mixed with lipid resonances for cells fed with LA) [16]. We also distinguish a component 5 located at or near the LDs with a spectral shape which is not of straightforward interpretation, and might be a result of image artifacts at the LDs. Indeed, distortions of the excitation fields by spatial refractive index structures lead to a modulation of the CARS intensity as discussed in [22] and might give rise to artifacts in the retrieved concentrations. As discussed in detail in our recent work [16], the error of the factorization in the FSC^3 analysis is quantified by the relative spectral error $\mathbf{E}_\mathrm{S}$ and the relative concentration error $\mathbf{E}_\mathrm{C}$. These are shown in Fig. 5 for the analysis reported in Fig. 4. The spectral error $\mathbf{E}_\mathrm{S}$ is a measure of the residual in the factorization of the phase-retrieved data set into the product of a matrix of concentrations and a non-negative matrix of spectra of the chemical components. The maximum relative spectral error in Fig. 5 is around 30% and is localized at large lipid droplets. The concentration error is defined as $\mathbf{E}_\mathrm{C} = \left\{ (\sum_{k=1}^{K} c_p^{\{k\}}) - 1 \right\}$ where $c_p^{\{k\}}$ is the non-negative relative volume concentration of the k-th chemical component at voxel p. Fig. 5 shows the spatial distribution of $\mathbf{E}_\mathrm{C}$, with largest relative errors located at the large lipid droplets and correlating with component 5, possibly due to distortions of the excitation fields by the spatial refractive index structure [22]. Note that the spatial-spectral coupling effects of the type described in [23] are expected to be weak if the resonant CARS contribution is much larger than the non-resonant one, which is the case in the CH stretch region and for droplets comparable or larger than the focal volume.

Interestingly, in cells fed with PA, smaller LDs (which tend to be located in the outer periphery of differentiated cells) exhibit a distinct lipid spectrum more resembling that of a saturated lipid such as PA (component 2 in the analysis, spatial distribution color–coded in green). Con-

#206105 - $15.00 USD Received 11 Feb 2014; revised 9 Mar 2014; accepted 9 Mar 2014; published 2 Apr 2014

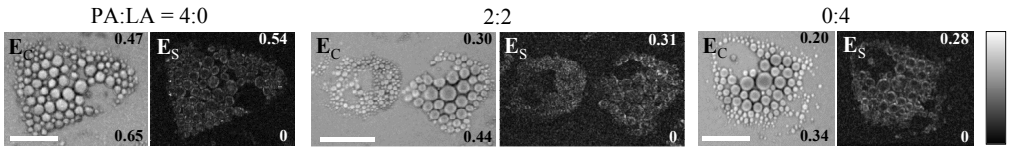

Fig. 5. Relative spectral error $\mathbf{E}_S$ and relative concentration error $\mathbf{E}_C$ for the same cells analyzed with FSC^3 in Fig. 4. The grey scale is indicated, with the range given for each image. The scale bars are 20 μm.

versely, large LDs formed during stem cell differentiation (also via LD fusion) and located toward the inner part of the cell appear to be filled with lipids from the differentiation media (mostly oleic acid). This finding suggests that PA in the supplemented medium is not easily transported across LDs during differentiation (possibly because of its lower fluidity, the melting temperature of PA is 63°) and remains located into smaller LDs. It is also interesting to see that the main lipid component in cells fed with the PA:LA mixture is well reproduced by an equally weighted combination of the LD spectrum of cells fed with LA and PA. As discussed above, the main lipid component in medium-large LDs of cells fed with PA appears to be the oleic-acid lipid present in the differentiation medium. Since both LA and oleic acid are liquid at room temperature, it is reasonable that they mix into a spatially homogeneous compound recognized as a single substance in the FSC^3 analysis. We also distinguish a more saturated lipid component in cells fed with the PA:LA mixture which is located in smaller LDs, similar to what observed in cells fed with PA only. No such component is observed in cells fed with LA only (which in fact are fully represented by 4 chemical components). As a side remark, we note that palmitic acid is the second most present fatty acid in human adipose tissue (21.5 %) after oleic acid (43.5 %), while α-linolenic acid is far less abundant (0.8 %) [21]. Despite being not so commonly present, our data suggest that α-linolenic acid is actually efficiently incorporated and stored in human adipocytes. Furthermore, the analysis of component 3 which appears more pronounced around LDs in cells fed with LA might suggest that LDs of different chemical composition have different protein coatings. This might be related to protein targeting mechanisms which are lipid specific. Indeed, how proteins target LDs is not yet well understood [4] and deserves more detailed studies.

For comparison, on the lower part of Fig. 4 we show the spatial distribution of the LD chemical content from a simple ratiometric analysis following the method by Rinia *et al.* [11]. We used the ratio of $\Im(\bar{\tilde{\chi}})$ between 2930/cm and 2855/cm representative of the lipid chemical composition through the degree of lipid disorder (which correlates with the degree of lipid chain unsaturation) as shown in Fig. 3 in the CH stretch region. The analysis shows the general trend of an increased degree of unsaturation going from cells fed with PA to cells fed with LA, but it offers far worse spatially-resolved chemical contrast than the results obtained with FSC^3.

4. Conclusions

In this work we have compared the performances of fast dual-frequency CARS imaging, requiring only minimal data analysis, with hyperspectral CARS imaging analyzed with phase-retrieval and an unsupervised factorization into concentrations of chemical components (FSC^3), for quantitative chemical imaging on human stem-cell derived adipocytes fed with saturated and poly-unsaturated fatty acids. We find that D-CARS is equally able to quantify the degree of poly-unsaturation when used in the fingerprint region. It is however less quantitative when used in the congested CH stretch region but still provides a qualitatively similar result as hyperspectral CARS. Hyperspectral CARS is specifically powerful when combined with FSC^3,

#206105 - $15.00 USD Received 11 Feb 2014; revised 9 Mar 2014; accepted 9 Mar 2014; published 2 Apr 2014

extracting the spatial distribution of chemical components with superior contrast compared to state-of-the-art ratiometric methods.

In view of the recently renewed interest in lipid droplet cell biology, these results pave the way towards label-free imaging of LDs with an unprecedented combination of subcellular spatial resolution, live cell dynamics and quantitative chemical sensitivity. This has the potential to answer many open questions on the fundamental molecular mechanisms of lipid metabolism in cells which might be of key importance to tackle metabolic disease, such as obesity and diabetes, which greatly effect today's modern societies.

Acknowledgment

This work was funded by the UK BBSRC Research Council (grant n. BB/H006575/1) and the UK EPSRC Research Council (grant n. EP/H045848/1). CDN acknowledges financial support by the President's Research Scholarship programme of Cardiff University and by the UK EPSRC Research Council (grant n. EP/I016260/1). PB acknowledges the UK EPSRC Research Council for her Leadership fellowship award (grant n. EP/I005072/1). FM acknowledges financial support from the European Union (Marie Curie Grant Agreement No. PERG08- GA-2010-276807).

#206105 - $15.00 USD Received 11 Feb 2014; revised 9 Mar 2014; accepted 9 Mar 2014; published 2 Apr 2014